Heliyon 7 (2021) e07682

Contents lists available at ScienceDirect

Heliyon

journal homepage: www.cell.com/heliyon

Research article

Comparative study on the effect of different copper loading on catalytic behaviors and activity of $Cu/ZnO/Al_2O_3$ catalysts toward CO and CO_2 hydrogenation

Tanutporn Kamsuwan, Chadaporn Krutpijit, Supareak Praserthdam, Suphot Phatanasri, Bunjerd Jongsomjit *, Piyasan Praserthdam

Center of Excellence on Catalysis and Catalytic Reaction Engineering, Department of Chemical Engineering, Faculty of Engineering, Chulalongkorn University, Bangkok 10330, Thailand

HIGHLIGHTS

- Comparative study of $Cu/ZnO/Al_2O_3$ (CZA) catalysts with different Cu loading in CO and CO_2 hydrogenation at 250 °C under atmospheric pressure was investigated.
- Results showed that methanol was the major product for CO hydrogenation, while the main product for CO_2 hydrogenation was CO.
- High Cu loading catalyst exhibited high catalytic activity in both CO and CO_2 hydrogenation.
- Low Cu loading catalyst showed deactivation with time on stream after 1–2 h by coke formation containing both amorphous and graphitic cokes for both CO and CO_2 hydrogenation.

ARTICLE INFO

Keywords:
CO
CO_2
Hydrogenation
Methanol production
$Cu/ZnO/Al_2O_3$ (CZA)
Cu loading amount

ABSTRACT

The ternary $Cu/ZnO/Al_2O_3$ (CZA) catalysts having different Cu loading were prepared by the co-precipitation method. Then, they were used in CO and CO_2 hydrogenation to produce methanol under atmospheric pressure at 250 °C. The high Cu loading CZA catalyst (CZA-H) resulted in the enhancement of structural features and textural properties (e.g., BET surface area and the crystallite size of copper species). Furthermore, the conversion of CO and CO_2 over CZA-H catalyst was apparently higher than that of the CZA-L (low Cu loading) catalyst. The major product of CO hydrogenation obtained from both catalysts was methanol, whereas in CO_2 hydrogenation, the main product was CO. Deactivation of catalysts was also crucial during CO and CO_2 hydrogenation. Therefore, the spent catalysts were determined to identify the nature of carbon formation. It revealed that amorphous and graphitic cokes were present. These cokes have different mechanisms in the elimination from the surface leading to influencing the deactivation process. The spent CZA-L was found to have higher carbon content, which was around 2.3% and 3.1% for CO and CO_2 hydrogenation, respectively. Besides the amorphous coke, the graphitic coke was also observed in CZA-L after time on stream for 5 h.

1. Introduction

At present, the environmental issues on the burning fossil fuels and results of certain chemical reactions in industrial factories such as cement manufactures have become concerned topics. For instance, the releasing of greenhouse gases into the atmosphere and the emission of poisoning gas (carbon monoxide) from the burning charcoal, running cars and the smoke from cigarettes, etc. essentially generate air pollution. The greenhouse gas such as CO_2 is the main environmental pollution for global warming. This problem leads to the utilization of carbonaceous feedstocks (CO and CO_2) in efficient ways to convert them into more valuable chemical products (Allam et al., 2019; Previtali et al., 2020). Hence, the study of high value-added products from the conversion of CO and CO_2 is interesting, especially on hydrogenation (Hu et al., 2018; Li et al., 2020). Synthesis of methanol from CO and CO_2 hydrogenation has been extensively studied because methanol is an important feedstock for several chemical productions that have widely application in the clean energy field including in chemical processes to produce products such as

* Corresponding author.
E-mail address: bunjerd.j@chula.ac.th (B. Jongsomjit).

https://doi.org/10.1016/j.heliyon.2021.e07682
Received 6 May 2021; Received in revised form 12 July 2021; Accepted 26 July 2021

fatty acid methyl ester (FAME), methyl tertiary butyl ether (MTBE), formaldehyde, acetic acid, methyl methacrylate, chloromethane and light olefin by methanol to olefin (MTO) process (Studt et al., 2012; Zuo et al., 2014; Liu et al., 2017; Xiao et al., 2017; Rafiee, 2020). Moreover, methanol can be used for fuel cell applications as the convenient storage of energy, especially in mobile devices and transportation. According to these reasons, the catalytic synthesis of methanol is still captivating. Methanol is normally produced from natural gas and coal, which mainly consist of CO, H_2, and a small amount of CO_2. Therefore, CO/CO_2 hydrogenation is a common process for methanol production via three reaction pathways (Pontzen et al., 2011; Pasupulety et al., 2015; Tursunov, 2017; Hu et al., 2018): CO hydrogenation [Eq. (1)], CO_2 hydrogenation [Eq. (2)], reverse water-gas shift (RWGS) reaction [Eq. (3)]. The involved reactions are as follows:

$$CO + 2H_2 \leftrightarrow CH_3OH \qquad \Delta H_{298K} = -90.84 \text{ kJ mol}^{-1} \tag{1}$$

$$CO_2 + 3H_2 \leftrightarrow CH_3OH + H_2O \qquad \Delta H_{298K} = -49.57 \text{ kJ mol}^{-1} \tag{2}$$

$$CO_2 + H_2 \leftrightarrow CO + H_2O \qquad \Delta H_{298K} = +41.27 \text{ kJ mol}^{-1} \tag{3}$$

The formation of methanol in both CO and CO_2 hydrogenation reactions [Eqs. (1) and (2)] is an exothermic reaction. These reactions likely undergo via low temperature under high pressure (An et al., 2007; Pasupulety et al., 2015; Tursunov, 2017). Many researchers reported that the methanol synthesis is operated at high pressure with moderate temperature (50–100 bar, 200–300 °C) by conventional CO and CO_2 hydrogenation (Studt et al., 2012; Pasupulety et al., 2015; Sadeghinia et al., 2020). The process of methanol formation at high pressure results in the cost of a mechanical process that is extremely high because of high energy consumption and must be installed more safety units to control the hazards in the methanol reaction process. Furthermore, the methanol yield in hydrogenation at low reaction temperature over the heterogeneous catalyst is very low that is related to the thermodynamic and the limit of reaction kinetics, in which it also shows the low catalytic activity. However, the increasing of reaction temperature leads to the formation of a large of undesired products. Therefore, the development of methanol synthesis under mild condition (low reaction pressure) in CO and CO_2 hydrogenation can decrease those problems, which is likely to be an important issue to improve the catalytic activity for producing of a purified desirable product and also results in saving the cost of production and technical issues in the manufacturing process (Bozzano and Manenti, 2016; Fang et al., 2019).

In addition, the catalysts play important roles to obtain high CO and CO_2 conversion, high selectivity and high stability via methanol synthesis in the hydrogenation. To avoid the undesired product, a chosen catalyst should be a neutral and basic function catalyst. The Cu-based catalyst is one of the most popular choices for industrial methanol production up on CO and CO_2 hydrogenation because it is easy to synthesize with low cost and high efficiency. Besides, the supported Cu catalysts promoted with metal oxides such as ZnO, ZrO_2, Ga_2O_3, B_2O_3, ZnO–Al_2O_3 and ZnO–ZrO_2 have been widely reported in order to improve the catalytic activity and selectivity of the product (Studt et al., 2012; Zhan et al., 2021). Over the past decades, the tertiary Cu/ZnO/Al_2O_3 (CZA) catalyst is dominant as a conventional catalyst to improve the catalytic performance that was reported in many researches (Guo et al., 2011; Zhang et al., 2011, 2012; Dasireddy and Likozar, 2019). The Cu is the main active site of tertiary catalyst, while ZnO can interact with H_2 adsorption by increasing the hydrogen spillover performance and support a Cu active site as a metal support effect. In general, Al_2O_3 is the third component of CZA catalyst used to increase the stability and activity of Cu/Zn component (Zhang et al., 2011; Liu et al., 2017). Moreover, some researchers suggested that methanol was directly formed via the interface of active site between copper and metal oxides in catalysts, whereas the reverse water-gas shift (RWGS) reaction was only taken place on the copper nanoparticles in catalysts (An et al., 2007; Tursunov, 2017; Li et al., 2020). The CZA catalyst is appropriate for methanol synthesis and it is more active in hydrogenation under high pressure. However, the deactivation is still a problem because the by-product formed during the hydrogenation can transform to coke and block the active surface leading to decreased catalytic activity (Ren et al., 2020). Besides, the depletion of metal oxide species arrangement (such as metal oxide dispersion) on the surface can also influence on the catalytic ability (Chu et al., 2013). According to the reasons above, the structure of catalyst and the nature of active species essentially affect the catalytic activity depending on the ratio of the copper, zinc and alumina. Therefore, the finding of suitable ratio of metal oxide (ZnO–Al_2O_3) and Cu support has been widely studied to obtain high conversion, selectivity, and recoverability (Pasupulety et al., 2015; Xiao et al., 2017; Dasireddy and Likozar, 2019; Zhan et al., 2021).

The aim of this work is to investigate the effect of Cu loading in the CZA catalysts synthesized by the co-precipitation method. The influence of Cu loading on CZA catalysts results in altering the structural catalyst and catalytic properties including active surface properties and catalytic performance. This research will bring about the alternative ways to reduce energy consumption and process cost. Therefore, the hydrogenation of CO and CO_2 under mild conditions (atmospheric pressure and 250 °C) for methanol production was performed. Furthermore, several characterization techniques such as XRD, SEM-EDX, ICP, XPS, H_2-TPR, CO_2-TPD and TGA were conducted to determine the physicochemical properties and active species on surface.

2. Experimental

2.1. Catalyst preparation

The tertiary Cu/ZnO/Al_2O_3 (CZA) catalysts with different copper (Cu) loading were prepared by the co-precipitation method. The two CZA catalysts having different weight ratios of Cu/Zn/Al that were 65/22/13 denoted as high amount of Cu content (CZA-H) and 39/49/12 denoted as low amount of Cu content (CZA-L) were synthesized. They were synthesized by using nitrate precursors including $Cu(NO_3)_2{\cdot}2.5H_2O$ (98.0%, Sigma-Aldrich), $Zn(NO_3)_2{\cdot}6H_2O$ (98.0%, Sigma-Aldrich) and $Al(NO_3)_3{\cdot}9H_2O$ (≥98.0%, Sigma-Aldrich). The mixture was dissolved in DI water at 80 °C. Then, sodium bicarbonate ($NaHCO_3$) solution was slowly added into the mixture for adjusting pH until the pH was 7. The mixture was stirred for 60 min at 80 °C and the metal complex precipitated. After this step, the precipitate solution was filtered and washed with deionized (DI) water until neutral. The obtained product in co-precipitation method was dried overnight at 110 °C and calcined under flowing of air at 350 °C for 3 h.

2.2. Catalyst characterization

The physico-chemical properties were identified by several techniques as follows;

X-ray diffraction (XRD) is the technique used to analyze crystal structure of these samples. The ternary structure of CZA catalysts was identified and collected on the X-ray diffractometer (SIEMENS D-5000 XRD) with CuK_α radiation (λ = 1.54439 Å). The XRD spectra were recorded under 2-theta degree in the range of 20°–80° at a scanning rate of 2.4° min^{-1}.

The N_2 physisorption technique was used to define the surface area by Brunauer-Emmett-Teller (BET) analysis, whereas average pore size and pore size distribution were calculated from the method of Barrett-Joyner-Halenda (BJH). The hysteresis loop (using the gas adsorption-desorption isotherms) of catalysts was obtained by a Micromeritics ASAP-2000 automated system. It was performed at -196 °C on a Micromeritics Chemisorb 2750 Pulse chemisorption system instrument. The CZA catalysts were degassed at 120 °C to remove the moisture and other adsorbates on the catalyst surface in a flowing of nitrogen at least 3 h before the measurements.

The morphologies were determined by scanning electron microscope (SEM) using a model of JEOL mode JSM-6400. Furthermore, the energy dispersive X-ray spectroscopy (EDX) was performed using Link Isis series 300 program to investigate the elemental distribution throughout the catalyst granules.

The quantity of elemental composition including copper, zinc and aluminum in bulk of the CZA catalysts was determined by inductively coupled plasma spectrometry (ICP). The ICP technique was used to analyze via digested catalyst with hydrochloric acid.

X-ray photoelectron spectroscopy (XPS) technique was used to analyze chemicals state of CZA catalysts by using the AMICUS spectrometer with MgK_α X-ray radiation (1253.6 eV) and AlK_α X-ray radiation (1486.6 eV) at voltage of 15 kV and current of 12 mA. The CZA catalyst was determined in 0–1200 eV. The Cu, Zn, Al, O, C species were detected by intensity and binging energy eV.

The reducibility and reduction temperature of the catalysts were analyzed by H_2 temperature-programmed reduction (H_2-TPR). This experiment was carried out in a continuous flowing system under atmospheric pressure using 0.05 g of catalyst and was heated at a temperature ramp from 40 to 600 °C at 10 °C/min. The reducing gas was 10% of H_2 in Ar.

Temperature-programmed desorption of carbon dioxide (CO_2-TPD) technique was used to measure the basicity of catalysts using carbon dioxide as the adsorbate. Approximately 0.10 g of catalyst was loaded and pretreated with 25 mL/min of helium at 250 °C for 30 min. The catalyst was adsorbed CO_2 at 40 °C for 1 h. Finally, the catalyst was heated up to 500 °C at a heating rate of 10 °C/min to desorb CO_2.

Thermal gravimetric analysis (TGA) was performed to measure the carbon deposition in the spent catalysts. The TGA was conducted using TA Instruments SDT Q 600 analyzer. The samples of 10–20 mg and a temperature ramp from 25 to 1000 °Cat 10 °C/min were used in the operation under flowing of air (400 ml/min).

2.3. Reaction test

The CZA-L or CZA-H catalyst of 0.1 g was packed into the fixed-bed continuous flow microreactor (O.D. 1.2 cm, I.D. 1.0 cm, height 50 cm) with 0.05 g of quartz wool. Firstly, the catalyst was pretreated under a flowing of N_2 at 250 °C for 30 min for moisture and impurity removal. Then, the catalyst was reduced under H_2 flow (40 ml/min) at 300 °C for 1 h to transform Cu oxides into Cu metal form. Finally, the catalytic hydrogenation of CO and CO_2 [gas hourly space velocity (GHSV) = 24,000 ml/g_{cat} h] was performed at the temperature of 250 °C under atmospheric pressure with time on stream for 5 h. For CO hydrogenation, the volume of CO:H_2 was 1:2 (balance with N_2), while CO_2 hydrogenation the volume of CO_2:H_2 is 1:3 (balance with N_2). The products of gas samples were analyzed by using gas chromatography (GC) with thermal conductivity detector (TCD, Shincarbon) to detect CO and CO_2 and flame ionization detector (FID, Rtx-5) to measure methanol.

The conversion of CO and CO_2 (X_i), selectivity of products (S_j) and yield of products (Y_j) represent the performance of catalysts. Then, we can demonstrate the catalytic activity of CO and CO_2 hydrogenation. All terms are calculated according to Eqs. (4), (5), and (6) as follows;

$$X_i(\%) = \frac{[n_i(\text{in}) - n_i(\text{out})] \times 100}{n_i(\text{in})} \quad (4)$$

$$S_j(\%) = \frac{n_j \times 100}{\sum n_j} \quad (5)$$

$$Y_j(\%) = \frac{X_i \times S_j}{100} \quad (6)$$

where n_i (in) is defined as the number of moles of CO or CO_2 in feed, n_i (out) is defined as the number of moles of unreacted CO or CO_2, and n_j is defined as the number of moles of each product.

3. Results and discussion

3.1. Catalyst characterization

The XRD patterns of CZA-H and CZA-L catalysts are shown in Figure 1. The XRD patterns for both catalysts are quite similar showing no peaks of malachite [$(Cu, Zn)_2(OH)_2CO_3$], which supposed to locate at 24.1° and 31.2° (Behrens et al., 2011; Jiang et al., 2019) and aurichalcite [$(Cu, Zn)_5(OH)_2CO_3$] with the expected characteristic peaks at 27.0 and 31.8° (Yang et al., 2018; Jiang et al., 2019), which were referred to the residue originating from the catalyst precursor without complete decomposition during the calcination process. On the other word, all residues were removed after calcination. Moreover, no specific peak of alumina was found in both catalysts because alumina may be presented as an amorphous species or it was in the highly disordered states, which results from the relatively low calcination temperature. However, both catalysts exhibited the main diffraction peaks of CuO phase at $2\theta = 35.6°$, 38.7°, 48.8°, 61.6° and 66.2° (Wang et al., 2011; Yang et al., 2018; Jiang et al., 2019), whereas the peaks at $2\theta = 31.7°$, 36.4°, 56.6°, 62.8° and 68.0° were assigned to ZnO phase in both CZA-H and CZA-L catalysts (An et al., 2007; Wang et al., 2011; Kou et al., 2019). It should be noted that the XRD patterns of CZA-L exhibited only the low intensity peaks of CuO, whereas the CZA-H not only showed strong intensity peaks of CuO, but also revealed some of ZnO species. This is obviously due to the higher amount of Cu present in CZA-H. Additionally, the average crystallite size of CuO was calculated by using Scherrer's equation using the CuO characteristic sharp peaks at $2\theta = 35.6°$, 38.7° and 48.8° and it is summarized in Table 1. The CuO crystallite size of CZA-L was smaller than CZA-H catalyst due to the large ZnO crystallites may cover some surfaces of CuO. Moreover, it is possible that the introduced CuO species is in low loading, and it is dispersed in the state of amorphous in the ZnO support (Ren et al., 2015; Hu et al., 2018). The morphology of catalysts was determined by SEM technique as shown in Figure 2. From SEM micrographs, it was found that the morphology of CZA-H catalyst granules is quite uniform than that of CZA-L catalyst. However, no significant differences in catalyst morphologies were observed from both CZA catalysts. In order to determine the elemental distribution near the surface of catalyst, EDX measurement was also performed along with SEM. The elemental distributions for Cu, Zn and Al of CZA catalysts are shown in Table 2 up on the expected and measured values. It should be noted that EDX measurement could evaluate the distribution of elements under surface (less than 5 microns). However, the EDX results revealed a good distribution of all elements compared with the expected values indicating the homogeneous elemental distribution throughout the catalyst granules.

In addition, the ICP-MS was also performed for elemental analysis in bulk catalyst. From ICP results (summarized in Table 2), the amounts of

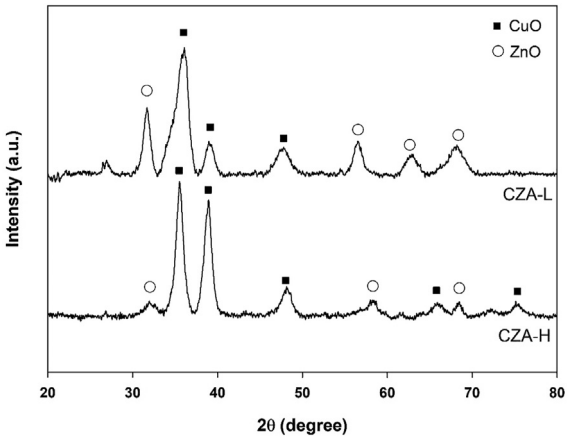

Figure 1. XRD patterns of CZA-L (Cu/Zn = 0.8) and CZA-H (Cu/Zn = 3.0) catalysts.

Table 1. Properties of CZA-L and CZA-H catalysts.

Catalyst	XRD d_{CuO} (nm)[a]	Surface area[b] (m^2/g)	Pore volume[c] (cm^3/g)	Pore size (nm)	Total Basicity (μmol CO_2/g)
CZA-L	4.9	49.5	0.3	16.9	88.9
CZA-H	8.7	77.5	0.5	17.4	77.3

[a] d_{CuO} was determined by the XRD data based on Scherrer's equation.
[b] Surface area was determined by BET method.
[c] Pore volume and pore size were determined by BJH desorption method.

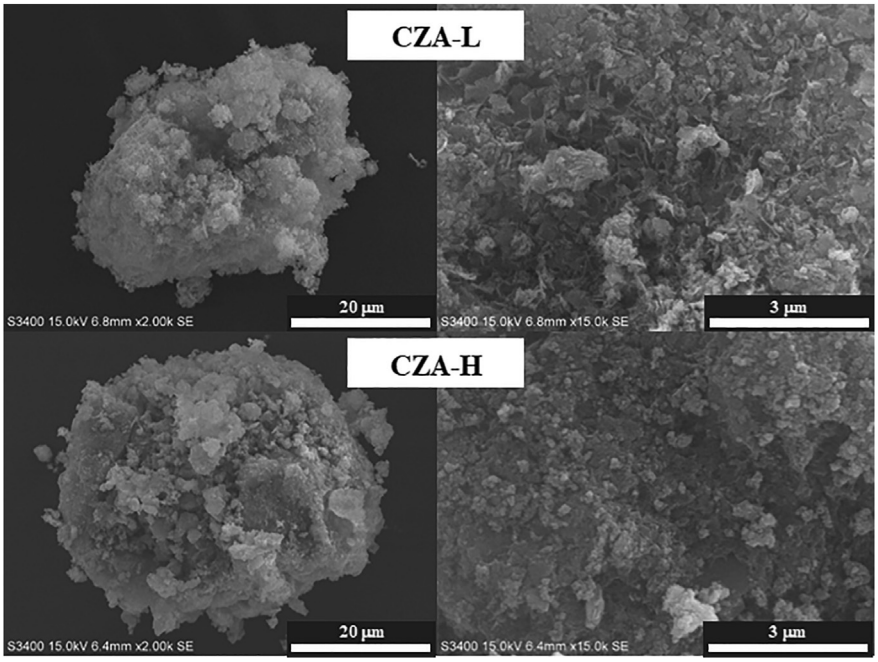

Figure 2. SEM image of CZA-L and CZA-H catalysts.

Table 2. Element distribution of CZA-L and CZA-H catalysts.

Element	CZA-L			CZA-H		
	Wt% (Expect)	EDX (Wt%)	ICP-MS (Wt%)	Wt% (Expect)	EDX (Wt%)	ICP-MS (Wt%)
Cu	39	42.3	35.8	65	70.0	71.8
Zn	49	53.0	59.7	22	24.5	24.5
Al	12	4.7	4.5	13	5.5	3.7
Cu/Zn	0.8	0.8	0.8	3.0	2.9	3.0

all elements in bulk catalyst are quite corresponding with those obtained from EDX measurements, especially for CZA-H. Moreover, the ratios of Cu/Zn calculated from both EDX and ICP-MS measurements were almost equal as expected in wt% of the catalyst preparation process, as seen in Table 2. The N_2 physisorption is a technique used to identify the BET surface area (S_{BET}) and pore structure of catalysts. The S_{BET}, pore volume (V_p) and pore size of catalysts are illustrated in Table 1. It is shown that S_{BET} of CZA-H (ca. 77.5 m^2/g) is higher than that of CZA-L catalyst (ca. 49.5 m^2/g). This is due to high Cu loading resulted in more generation of porous structure. Considering the pore structure of catalysts, the high Cu loading in CZA catalyst provided the high V_p (ca. 0.5 cm^3/g) and a slight difference of pore size diameter as seen in Table 1. Furthermore, the average pore size diameter of CZA catalysts was in the range of mesoporous structure (2–50 nm) with having an average pore size of approximately 17 nm.

The XPS is one of the most powerful technique that was performed to analyze the chemical state of CZA catalysts. The XPS spectra for Cu species of fresh CZA catalysts (Figure 3) were observed at 935.6 ± 0.3 eV and 954.9 ± 0.7 eV, which were attributed to the binding energy (BE) of Cu $2p_{3/2}$ and Cu $2p_{1/2}$ in the state of Cu^{2+} for excite state in form of Cu^0 ($Cu^{2+} \rightarrow Cu^0$). It acted as the main active site of CO and CO_2 hydrogenation. Moreover, the shake-up Cu 2p satellite peaks were located at 944.9 ± 0.3 eV and 963.9 ± 0.2 eV. According to Ahmad et al. (2014) and Li et al. (2019), they reported that Cu $2p_{3/2}$ and Cu $2p_{1/2}$ corresponded to the presence of Cu^{2+} ions of cupric oxide in CZA catalysts. Furthermore, the binding energy of satellite peaks can be confirmed that the catalyst surface was filled with the existence of Cu^{2+} without Cu^+ species. As a result, the different Cu loading affected the amount of Cu^{2+} on catalyst surface by following a peak of Cu $2p_{1/2}$ and Cu $2p_{3/2}$. However, these peaks for CZA-L catalyst shifted to lower binding energy, indicating the presence of high amount of Zn content. It was probably attributed to the effect of electron transformation and the interaction between Cu and Zn species (Cai et al., 2021). In addition, the peaks around ≈1023 eV (Zn $2p_{3/2}$) and ≈1046 eV (Zn $2p_{1/2}$) are assigned to the existence of Zn^{2+} species on catalyst surface (Mousavi-Kamazani, 2019). The binding energy of Al 2p was detected at ca. 78 eV, corresponding to the Al^{3+} species dispersed on surface of CZA catalysts (Ahmad et al., 2014; Xiao et al., 2017).

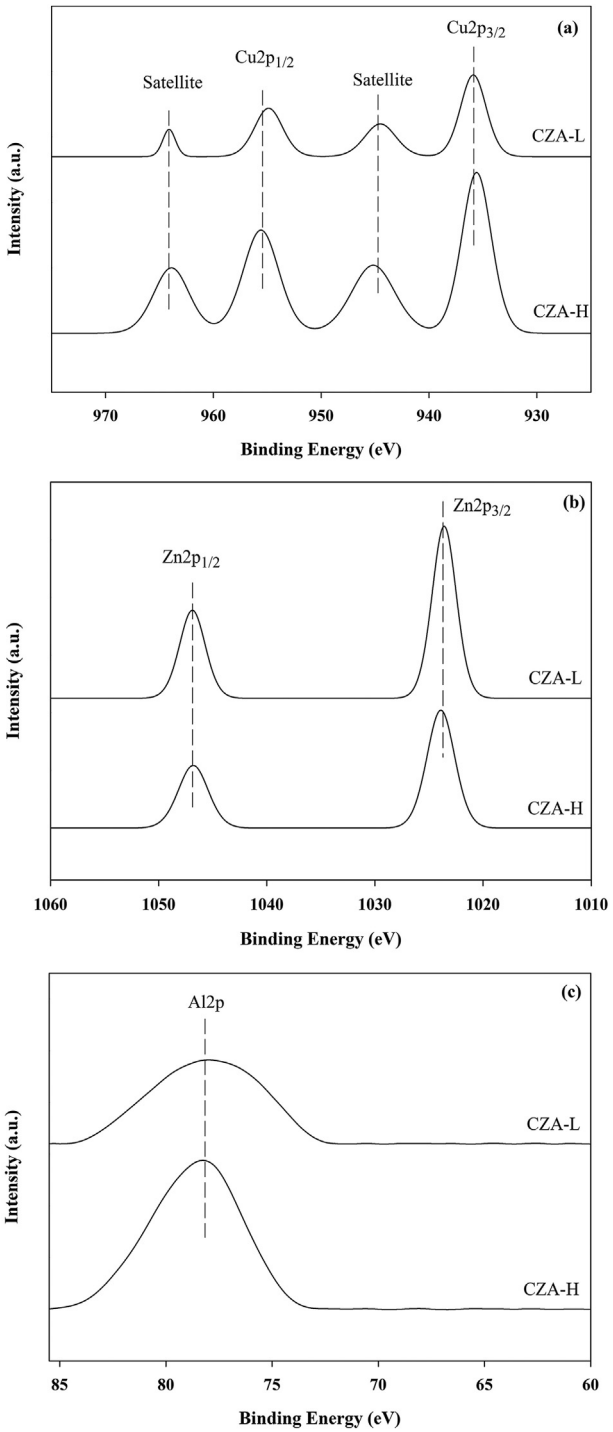

Figure 3. XPS signals of CZA-L and CZA-H catalysts (a) XPS of Cu species, (b) XPS of Zn species and (c) XPS of Al species.

The temperature-programmed reduction (TPR) is a key technique to determine the reduction behaviors of catalysts. The H_2-TPR profiles of CZA catalysts are presented in Figure 4. The result in TPR profile showed that the characteristics peak appeared in the temperature ranging from 220 to 275 °C, corresponding to the reduction of different CuO species as follows. Firstly, the reduction of highly dispersed copper oxides (CuO) was observed at the low temperature reduction peak (α peak) (Zhang et al., 2018; Dasireddy and Likozar, 2019). Secondly, high temperature reduction (β peak) indicated the reduction of bulk CuO (Zhang et al., 2018; Dasireddy and Likozar, 2019). The TPR profile of CZA-H showed

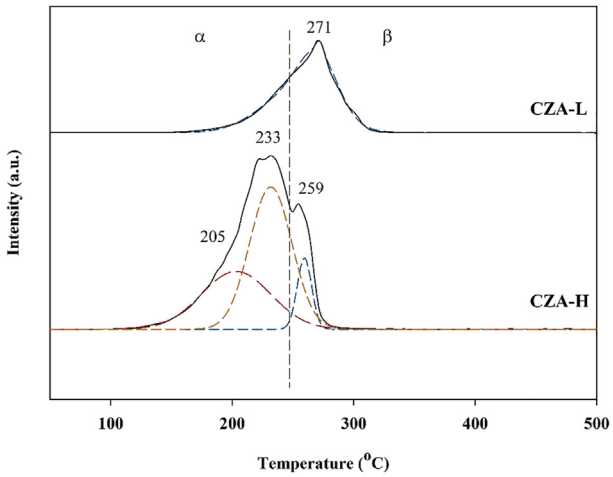

Figure 4. H_2-TPR profile of CZA-L and CZA-H catalysts.

two major reduction peaks at low temperature for α peak including peaks at 205 °C and 233 °C that were attributed to the CuO dispersion and direct interaction between CuO species and ZnO species (Hu et al., 2018; Sadeghinia et al., 2020). Moreover, the high temperature reduction peak (ca. 259 °C) of CZA-H catalyst can be ascribed to an interaction of isolated copper oxides (CuO) in bulk ZnO (Yang et al., 2008; Panyad et al., 2011). In contrast, CZA-L catalyst showed only one sharp peak with shoulder at high temperature (ca. 271 °C) corresponded to a strong interaction between CuO and ZnO and core layer of CuO (bulk-core CuO), resulting in an increase in the reducibility of CuO (Panyad et al., 2011; Zhang et al., 2011). The reduction peak of CuO shifted to the higher temperature and tended to be narrower with increasing zinc content as well as the TPR result of CZA-L with low Cu content compared to CZA-H catalyst. This can also illustrate that the crystallite size of CuO decreased in CZA-L (Table 1) because the small crystallite size of CuO is consistent with high reduction temperature (Dasireddy and Likozar, 2019). However, the reduction of ZnO species did not appear under this experimental condition because it occurred at very high temperature (Zhan et al., 2014). Furthermore, the reduction peak contributions regarding to the TPR patterns of the investigated catalysts are summarized in Table 3. The relative contribution in the range of low temperature peak (α peak) over CZA-H is 90.7%, whereas the CZA-L did not appear the peak contribution at low temperature. This result indicates that the amount of dispersed CuO over CZA-H is much higher than CZA-L, and it is also confirmed with XRD analysis as shown in Figure 1.

The basic properties of catalyst are also important to identify since CO and CO_2 can be well adsorbed on the basic sites. Thus, the CO_2-TPD was performed to determine the basicity of CZA catalysts. As known, the basic properties of catalysts can be divided into two types of basic site by a different range of CO_2 desorption temperature such as weak and moderate to strong basic site (Zhang et al., 2011; Tursunov et al., 2017; Zhang et al., 2017). The weak basic sites (low desorption temperature) were assigned to the structural OH groups on surface catalysts, while moderate to strong basic sites (high desorption temperature) were related to metal-oxygen pairs and the coordinately unsaturated O^{2-} ions (Zhang et al., 2017; Dasireddy et al., 2018). The desorption peaks of CO_2 (CO_2-TPD profiles) of catalysts are illustrated in Figure 5. The CZA catalysts showed only one characteristic CO_2 desorption peak, which was referred to weak basic sites of CZA catalysts. It can be ascribed to weak basic sites that were dominant for CZA catalysts for both low and high Cu loading in this case. In addition, the number of basic sites (total basic site) on catalyst is also reported in Table 1. It can be calculated by integration of CO_2 desorption peak area according to the Gauss curve fitting method. The total basic sites of CZA-L (ca. 88.9 μmol CO_2/g_{cat}) were slightly higher than CZA-H (ca. 77.3 μmol CO_2/g_{cat}). As known, the nature of the basicity on catalyst surface is different depending on the presence of

Table 3. H_2 reduction peak contributions of the CZA catalysts in the temperature-programmed reduction (TPR).

Catalyst	$T_{\alpha1,\ \alpha2}$ (°C)	T_β (°C)	% of Aα[a]	% of A_β[b]
CZA-L	205, 233	259	90.7	9.3
CZA-H	-	271	-	100

[a] The relative contribution of α peak.
[b] The relative contribution of β peak.

different ratios of Cu/Zn content in CZA catalysts, which affects the CO and CO_2 hydrogenation regime for methanol synthesis.

3.2. Hydrogenation reaction test

The catalytic hydrogenation of CO and CO_2 over CZA-L and CZA-H catalysts was performed to measure the catalytic activity in terms of CO and CO_2 conversion at 250 °C under atmospheric pressure. The catalytic performance of CZA catalysts was determined under time on stream (TOS) of 5 h as shown in Figure 6(a) and Figure 6(b) for CO and CO_2 hydrogenation, respectively. The results of CO conversion [Figure 6(a)] showed that CZA-H catalyst exhibited similar behavior with CZA-L during 2 h (CO conversion ≈1.4%), and then the CO conversion of CZA-L apparently decreased to 0.9%, whereas the CZA-H was quite stable. In other words, CZA-L exhibited deactivation of catalyst after being used for 5 h. Considering the CO_2 hydrogenation [Figure 6(b)], the CO_2 conversion of CZA-H increased up to 4%, and then dropped to 3% after being used for 5 h. In contrast, CZA-L showed higher CO_2 conversion of 3% at the beginning of reaction test, and then it decreased to 1% after being used for 1 h. However, higher CO and CO_2 conversions were obtained from CZA-H, in which the CO and CO_2 conversions reached constant value of ca. 2% and 3%, respectively with increasing the reaction time from initial to 5 h (as seen in Table 4). This is probably due to high surface area of CZA-H (S_{BET}, as seen in Table 1), high Cu loading and high dispersion of CuO in CZA-H (Cu/Zn = 3.0) as expected, which promote the contact between H_2 and CO or CO_2 over the Cu active site leading to an increase in catalytic activity. According to several reports, they proposed that Cu^0 sites act as the main active sites in the adsorption and dissociation of H_2, CO and CO_2, which are favorable in the hydrogenation reaction (Gao et al., 2013; Liu et al., 2017; Okemoto et al., 2020). Meanwhile, having a large amount of Zn on the Cu supported catalyst (CZA-L, Cu/Zn = 0.8) led to decrease the catalytic performance in the CO and CO_2 hydrogenation reaction by agglomeration of ZnO particles, resulting in blockage of the active site of catalyst and loss of active surface site (Fichtl et al., 2015; Chiang et al., 2018). However, the role of ZnO species is to improve the dispersion and number of active copper metal site. Therefore, this finding of the optimal ratio of Cu/Zn in CZA

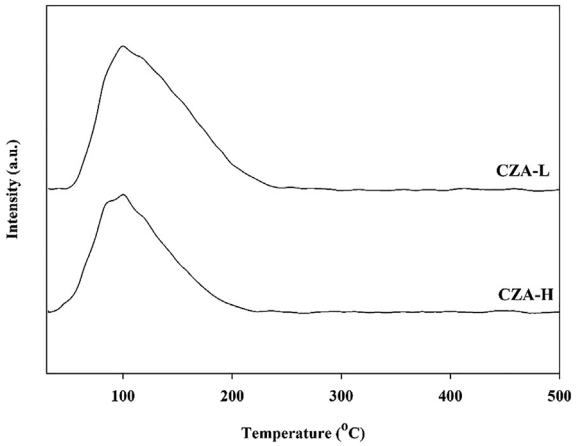

Figure 5. CO_2-TPD profile of CZA-L and CZA-H catalysts.

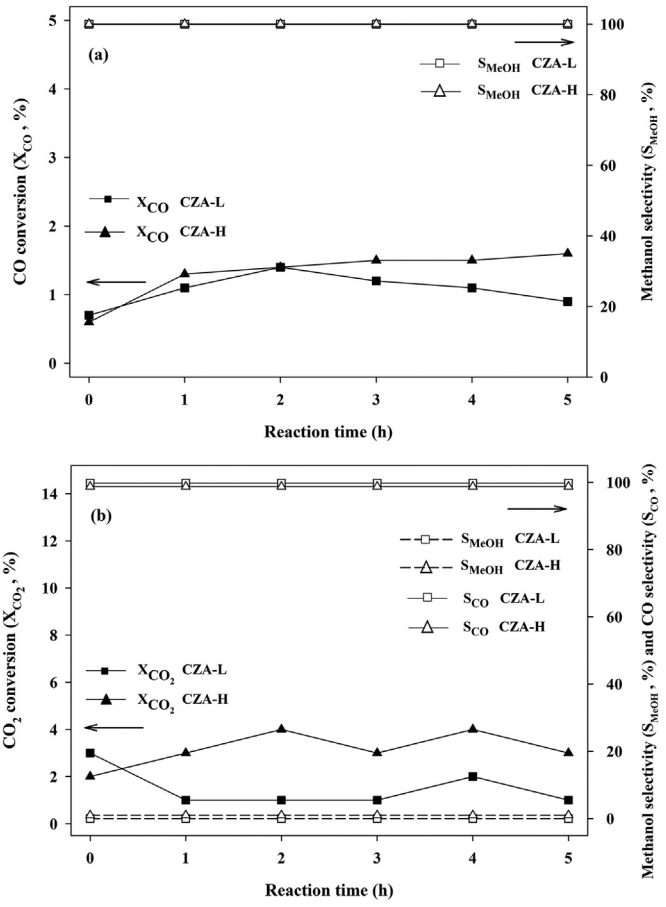

Figure 6. Catalytic activity of CZA-L and CZA-H at different feedstocks at 250 °C under atmospheric pressure. (a) CO hydrogenation and (b) CO_2 hydrogenation.

catalyst is important to enhance the catalytic activity (Chiang et al., 2018). From these results, the ratio of Cu/Zn is 3.0 (CZA-H) having the optimum interface site of the ZnO–Cu exhibited higher catalytic activity. Considering the deactivation of catalyst, it was found that the activity of CZA-L decreased with time on stream after 1–2 h during CO hydrogenation due to the migration of metal species and coke formation on the catalyst surface (Okemoto et al., 2020). Meanwhile, the CZA-H catalysts showed better stability. Both CO and CO_2 conversions over the CZA-L and CZA-H catalysts are relatively low compared to other researches. Previously, some researchers studied on CO and CO_2 hydrogenation reaction at medium to high pressure (over 2 MPa) and they reported the CO conversion in the range of 5–12%, depending on pressure and temperature of reaction (Previtali et al., 2020; Sadeghinia et al., 2020). In case of CO_2 hydrogenation, they reported the conversion of CO_2 under moderate pressure (over 5 MPa) that is around 7–16% (Sun et al., 2015; Sadeghinia et al., 2020). From these observations, it can be illustrated that the conversion of CO and CO_2 is not relatively high because methanol synthesis is severely limited by thermodynamics and more influence of condition reaction. Therefore, we can simply screen the catalyst that has good surface properties and suitable of metal oxide arrangement on active surface in the hydrogenation reaction under specific conditions.

Both CZA-L and CZA-H catalysts produced only methanol from CO hydrogenation [ca. 100% selectivity, as seen in Figure 6(a)], which is promising. Meanwhile, CO_2 hydrogenation with these two catalysts only produced CO as the main product [Figure 6(b)]. This is probably because the CO_2 can be easily converted to CO under this condition via RWGS reaction rather than CO_2 hydrogenation reaction to methanol. In fact, methanol is formed from CO when the surface is majorly

Table 4. CO and CO_2 conversion and product selectivity obtained from the hydrogenation reaction at 250 °C under atmospheric pressure.

Catalysts	Reaction time 5 h				
	CO hydrogenation		CO_2 hydrogenation		
	CO conversion (%)	Methanol Selectivity (%)	CO_2 conversion (%)	CO Selectivity (%)	Methanol Selectivity (%)
CZA-L	1	100	1	100	0
CZA-H	2	100	3	99	1

covered by Cu^0 sites, according to the methanol synthesis. According to the proposed mechanism in Figure 7, the interaction of Cu^0 sites with different feedstocks between CO and CO_2 in hydrogenation reaction leads to the formation of dissimilar product distribution (methanol and CO, as seen in Figure 6). Based on some researches (Fujita et al., 1995; Allam et al., 2019), they reported that the methanol formation is produced from the CO hydrogenation in the process of methoxy species creation (formyl pathway) to form methanol as the main product in CO hydrogenation. However, CO_2 hydrogenation over Cu-based catalysts will produce CO (RWGS reaction) via the dissociation reaction of CO_2 and it can generate the Cu–O–Cu species on the surface (carboxyl intermediate pathway). The mechanism of the reaction intermediate for adsorbed species on Cu-based catalysts is also supported by other researches (Gogate, 2019; Guil-López et al., 2019). Moreover, this reaction generates the surface hydroxyl species, and then it decomposes into water molecule that is the main reason in the inhibition of active sites for the methanol formation (Allam et al., 2019; Guil-López et al., 2019). From this point of view, the catalytic activity of carbon monoxide to methanol depended on the amount of Cu^0 sites (Gao et al., 2013; Liu et al., 2017). In other words, the RWGS can occur in CO_2 hydrogenation via the reduction of CO_2 to CO over the Cu site in catalyst under atmospheric condition. Moreover, the Cu supported catalyst shows high stability, high activity with small amount of undesired products formation in the condition having large amount of CO_2 in feed. The Cu site is able to increase the catalytic performance under atmospheric pressure at low temperature for RWGS reaction (Elsernagawy et al., 2020). This is because CO_2 in feed can adsorb on the surface under oxidation and reduction of the Cu supported catalysts (Elsernagawy et al., 2020; Okemoto et al., 2020). Hence, it can be suggested that Cu supported catalyst ($Cu/ZnO/Al_2O_3$) exhibits good performance for the RWGS reaction at a lower temperature under atmospheric pressure. From our observation in this stage, it can be deduced that CZA-H is a good potential catalyst for CO hydrogenation to methanol and CO_2 reduction to CO under this specified condition.

3.3. The deactivation of spent catalysts

The total amount of carbon deposition on CZA catalysts after being used in CO and CO_2 hydrogenation at 250 °C under atmospheric pressure for 5 h was analyzed by the thermogravimetric analysis (TGA, as seen in Figure 8) with heating temperature ranging from room temperature to 1000 °C. Figure 8(a) shows TGA profiles of the spent catalysts from CO hydrogenation and Figure 8(b) represented TGA profiles of the spent catalysts from CO_2 hydrogenation. It can be observed that all catalysts exhibited similar weight loss behavior after hydrogenation test. The weight losses of CZA-L and CZA-H catalysts in the temperature range of 300–600 °C were used to explain the amount of carbon content from the burning of coke implanted on the catalyst surface (Zhuang et al., 2019; Ren et al., 2020). Considering the CO hydrogenation, the amount of coke on the surface of catalysts was 0.8% and 2.3% for the spent CZA-H and CZA-L, respectively. In addition, the spent CZA-H showed the amount of coke of 0.9%, whereas 3.1% of coke was obtained from the spent CZA-L after CO_2 hydrogenation test. In both cases of CO and CO_2 hydrogenation, CZA-H catalyst exhibited lower coke deposition than CZA-L. According to the TGA analysis and catalytic activity results, it was suggested that the CZA-L catalyst with high ZnO content can migrate and generate the graphitic coke to block the active sites (Liang et al., 2019; Laudenschleger et al., 2020; Okemoto et al., 2020). Furthermore, large amounts of carbon deposition over CZA catalysts were formed by the decomposition of CO and CO_2 molecules with the reduction of ZnO and CuO, and Cu oxidation (Chiang et al., 2018), which was related to low catalytic activity as shown in Figure 6. It is well known that the species of carbon content can be generally divided into two groups depending on the range of temperature: (1) amorphous carbon or soft coke (at low temperature); and (2) graphitic carbon or hard coke (at high temperature). The

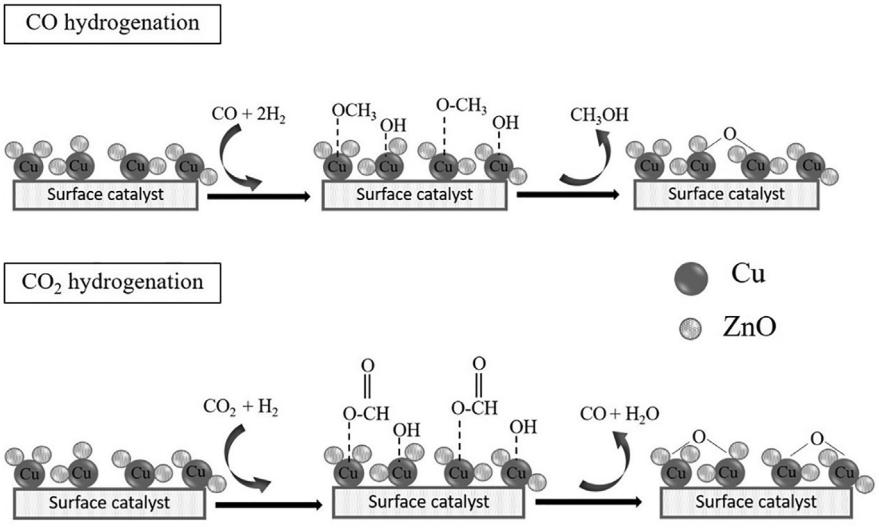

Figure 7. Proposed mechanism for the CO and CO_2 hydrogenation over Cu-based catalyst.

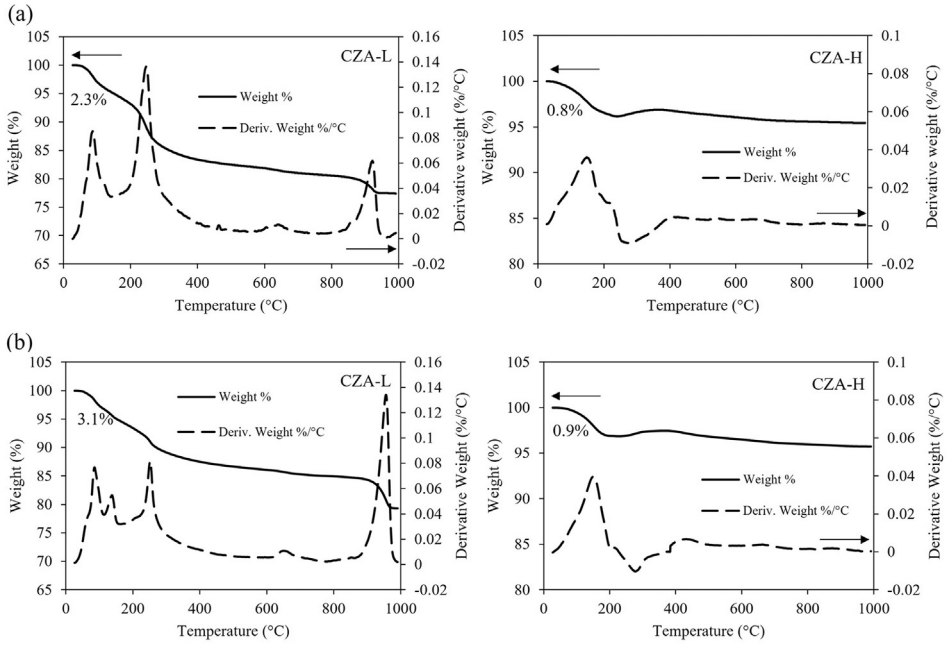

Figure 8. TGA analysis of spent catalysts: (a) spent CZA-L and CZA-H catalysts after being used for 5 h in CO hydrogenation and (b) spent CZA-L and CZA-H catalysts after being used for 5 h in CO_2 hydrogenation.

amorphous carbon on the catalyst surface can be easily eliminated by oxidation or hydrogen reduction and can be also converted to graphitic coke. The graphitic carbon (hard coke) on the catalyst surface is extremely difficult to remove leading to complete deactivation (Argyle and Bartholomew, 2015; Chen et al., 2020). Considering the derivative weight as also shown in Figure 8, the types of coke present on the spent CZA-L and CZA-H can be elucidated. It can be observed that both spent CZA catalysts exhibited similar derivative weight patterns for both CO and CO_2 hydrogenation. The spent CZA-L catalyst exhibited three groups of peaks: (1) the peak at a below temperature 200 °C assigned to the removal of moisture; (2) the peak in the temperature range of 200–400 °C representing the removal of amorphous coke; and (3) the peak over 900 °C revealing the graphitic cokes. It is obviously observed that the graphitic coke was not present in the spent CZA-H catalyst in both CO and CO_2 hydrogenation. This is probably because the formation of coke was affected by different copper loading or Cu dispersion. Moreover, Pampararo et al. (2020) and Wu et al. (2021) suggested that the high amount of Cu loading provided the improvement of the oxidation of carbonaceous materials (amorphous carbon and graphitic carbon species) over the catalyst surface, in which these carbon species were eliminated by activating of oxygen on the catalyst surface. This may be the reason why the CZA-H exhibited higher activity and the CZA-L resulted in fast deactivation because of the formation of graphitic coke. In order to analyze the surface morphology, SEM/EDX analysis was used to identify the morphology and the relative percentage of elemental distribution in both CZA catalysts after reaction testing as shown in Figure 9 and Table 5, respectively. From SEM results of spent CZA catalyst (Figure 9), it can be observed that CZA-H can retain the similar morphology as compared to its fresh catalyst in both CO and CO_2 hydrogenation, while CZA-L exhibited more fibrous like structure on the external surface after being used due to higher amount of coke. The EDX analysis was used to determine an elemental distribution on catalyst by scattering technique and presented in percent weight of each element (referred to Table 5). The amounts of carbon (C) presented as coke formation in different spent catalysts were observed. It revealed that the carbon content apparently decreased in the following order; CO-CZA-H <

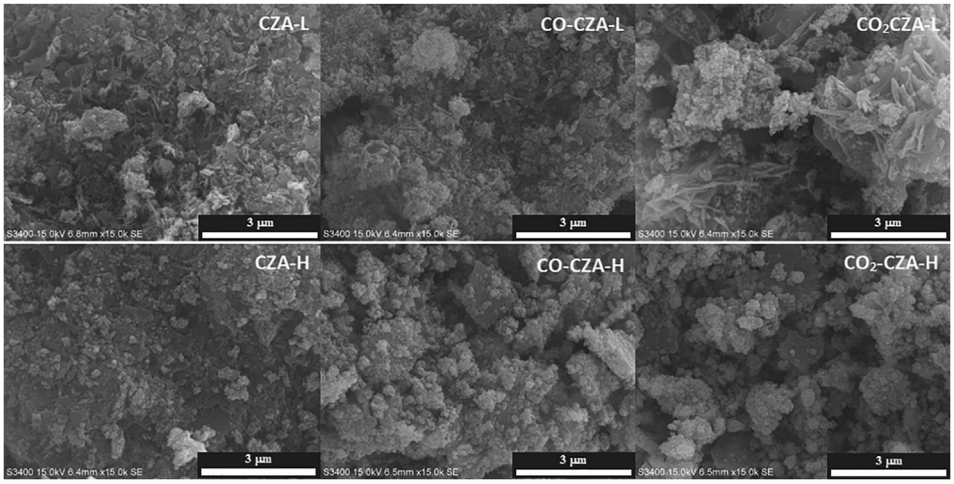

Figure 9. SEM images of spent CO-CZA-L, CO-CZA-H, CO_2-CZA-L and CO_2-CZA-H catalysts.

Table 5. Relative weight percentage of elements distribution in spent CZA catalysts from CO and CO_2 hydrogenation reaction at 250 °C under atmospheric pressure.

Element	Weight percentage of element (wt%)			
	CO hydrogenation		CO_2 hydrogenation	
	CO-CZA-L	CO-CZA-H	CO_2-CZA-L	CO_2-CZA-H
Copper (Cu)	41.2	68.3	40.4	68.8
Zinc (Zn)	51.9	24.9	50.1	24.7
Aluminium (Al)	4.0	5.4	5.2	4.7
Carbon (C)	2.9	1.4	4.3	1.8

CO-CZA-L in CO hydrogenation as same as CO_2-CZA-H < CO_2-CZA-L in CO_2 hydrogenation. Interestingly, the carbon content in spent catalysts referred to the coke formation after being used in CO and CO_2 hydrogenation and resulted in deactivation of catalyst. Therefore, CZA-H exhibited lower carbon content that inferred the high stability (as presented in Figure 6). Based on these results, it concludes that CZA-L is possibly deactivated, which is related to decreased stability (as seen in Figure 6). The EDX measurement results are also corresponding with those obtained from TGA analysis as mentioned earlier.

The relationship among the weight ratio of Cu/Zn, conversion, basic sites, and coke deposition was elucidated. It was found that CZA catalyst having high Cu/Zn ratio (high Cu loading) showed higher catalytic activity and lower coke deposition (TGA result). On the other hand, the increased amount of Zn content (Cu/Zn ratio is low) resulted in a decrease in the conversion of CO and CO_2. In summary, the activity of CZA catalysts from our studies (under mild condition) is not relatively high as compared with other reports, but we are able to apply this condition for the catalyst screening. Moreover, the different deactivation pathways can be observed depending on differences in Cu loading under the CO and CO_2 hydrogenation.

4. Conclusion

The effect of different Cu loading in a ternary Cu/ZnO/Al_2O_3 (CZA) catalysts including CZA-H (ratio of Cu/Zn = 3.0) and CZA-L (ratio of Cu/Zn = 0.8) synthesized by the co-precipitation method was investigated in both CO and CO_2 hydrogenation. The mild hydrogenation condition (250 °C and atmospheric pressure) was applied for the catalyst screening. The results indicated that the CZA-H (high Cu loading) exhibited higher catalytic activity in both CO and CO_2 hydrogenation when compared to CZA-L (low Cu loading). For both catalysts, methanol can be potentially produced by CO hydrogenation, whereas only CO formation was obtained from CO_2 hydrogenation. The stability test revealed that both catalysts exhibited different deactivation pathways. It was found that the graphitic coke was present only in the spent CZA-L catalyst for both CO and CO_2 hydrogenation.

Declarations

Author contribution statement

Tanutporn Kamsuwan: Conceived and designed the experiments; Performed the experiments; Analyzed and interpreted the data; Wrote the paper.

Chadaporn Krutpijit: Performed the experiments.

Supareak Praserthdam & Piyasan Praserthdam: Contributed reagents, materials, analysis tools or data.

Suphot Phatanasri: Conceived and designed the experiments.

Bunjerd Jongsomjit: Conceived and designed the experiments; Wrote the paper.

Funding statement

This work was supported by Ratchadapisek Somphot Fund for Postdoctoral Fellowship, Chulalongkorn University, and also by the Malaysia-Thailand Joint Authority (MTJA).

Data availability statement

Data included in article/supp. material/referenced in article.

Declaration of interests statement

The authors declare no conflict of interest.

Additional information

No additional information is available for this paper.

Acknowledgements

This research is supported by Ratchadapisek Somphot Fund for Postdoctoral Fellowship, Chulalongkorn University. The authors also would like to thank Malaysia-Thailand Joint Authority (MTJA) for supporting this research.

References

Ahmad, R., Hellinger, M., Buchholz, M., et al., 2014. Flame-made Cu/ZnO/Al_2O_3 catalyst for dimethyl ether production. Catal. Commun. 43, 52–56.

Allam, D., Cheknoun, S., Hocine, S., 2019. Operating conditions and composition effect on the hydrogenation of carbon dioxide performed over CuO/ZnO/Al_2O_3 catalysts. Bull. Chem. React. Eng. Catal. 14 (3), 604–613.

An, X., Li, J., Zuo, Y., et al., 2007. A Cu/Zn/Al/Zr fibrous catalyst that is an improved CO_2 hydrogenation to methanol catalyst. Catal. Lett. 118 (3), 264–269.

Argyle, M.D., Bartholomew, C.H., 2015. Heterogeneous catalyst deactivation and regeneration: a review. Catalysts 5 (1).

Behrens, M., Brennecke, D., Girgsdies, F., et al., 2011. Understanding the complexity of a catalyst synthesis: Co-precipitation of mixed Cu,Zn,Al hydroxycarbonate precursors for Cu/ZnO/Al_2O_3 catalysts investigated by titration experiments. Appl. Catal. Gen. 392 (1), 93–102.

Bozzano, G., Manenti, F., 2016. Efficient methanol synthesis: perspectives, technologies and optimization strategies. Prog. Energy Combust. Sci. 56, 71–105.

Cai, X., Ke, Y., Wang, B., et al., 2021. Efficient catalytic amination of diols to diamines over Cu/ZnO/γ-Al_2O_3. Mol. Catal. 508, 111608.

Chen, F., Tao, Y., Ling, H., et al., 2020. Ni-cu bimetallic catalysts on yttria-stabilized zirconia for hydrogen production from ethanol steam reforming. Fuel 280, 118612.

Chiang, C.-L., Lin, K.-S., Chuang, H.-W., 2018. Direct synthesis of formic acid via co2 hydrogenation over Cu/ZnO/Al_2O_3 catalyst. J. Clean. Prod. 172, 1957–1977.

Chu, Z., Chen, H., Yu, Y., et al., 2013. Surfactant-assisted preparation of Cu/ZnO/Al_2O_3 catalyst for methanol synthesis from syngas. J. Mol. Catal. Chem. 366, 48–53.

Dasireddy, V.D.B.C., Neja, S.Š., Blaž, L., 2018. Correlation between synthesis ph, structure and Cu/MgO/Al_2O_3 heterogeneous catalyst activity and selectivity in CO_2 hydrogenation to methanol. J. CO_2 Util. 28, 189–199.

Dasireddy, V.D.B.C., Likozar, B., 2019. The role of copper oxidation state in Cu/ZnO/Al_2O_3 catalysts in CO_2 hydrogenation and methanol productivity. Renew. Energy 140, 452–460.

Elsernagawy, O.Y.H., Hoadley, A., Patel, J., et al., 2020. Thermo-economic analysis of reverse water-gas shift process with different temperatures for green methanol production as a hydrogen carrier. J. CO_2 Util. 41, 101280.
Fang, X., Men, Y., Wu, F., et al., 2019. Moderate-pressure conversion of H_2 and CO_2 to methanol via adsorption enhanced hydrogenation. Int. J. Hydrogen Energy 44 (39), 21913–21925.
Fichtl, M.B., Schlereth, D., Jacobsen, N., et al., 2015. Kinetics of deactivation on Cu/ZnO/Al_2O_3 methanol synthesis catalysts. Appl. Catal. Gen. 502, 262–270.
Fujita, S., Usui, M., Ito, H., et al., 1995. Mechanisms of methanol synthesis from carbon dioxide and from carbon monoxide at atmospheric pressure over Cu/ZnO. J. Catal. 157 (2), 403–413.
Gao, P., Li, F., Zhang, L., et al., 2013. Influence of fluorine on the performance of fluorine-modified Cu/Zn/Al catalysts for CO_2 hydrogenation to methanol. J. CO_2 Util. 2, 16–23.
Gogate, M.R., 2019. Methanol synthesis revisited: reaction mechanisms in CO/CO_2 hydrogenation over Cu/ZnO and dft analysis. Petrol. Sci. Technol. 37 (5), 603–610.
Guil-López, R., Mota, N., Llorente, J., et al., 2019. Methanol synthesis from CO_2: a review of the latest developments in heterogeneous catalysis. Materials 12 (23).
Guo, X., Mao, D., Lu, G., et al., 2011. CO_2 hydrogenation to methanol over Cu/ZnO/ZrO_2 catalysts prepared via a route of solid-state reaction. Catal. Commun. 12 (12), 1095–1098.
Hu, X., Qin, W., Guan, Q., et al., 2018. The synergistic effect of cuznceox in controlling the formation of methanol and CO from CO_2 hydrogenation. ChemCatChem 10, 4438–4449.
Jiang, X., Chen, X., Ling, C., et al., 2019. High-performance Cu/ZnO catalysts prepared using a three-channel microreactor. Appl. Catal. Gen. 570, 192–199.
Kou, J.-W., Cheng, S.-Y., Gao, Z.-H., et al., 2019. Synergistic effects of potassium promoter and carbon fibers on direct synthesis of isobutanol from syngas over Cu/ZnO/Al_2O_3 catalysts obtained from hydrotalcite-like compounds. Solid State Sci. 87, 138–145.
Laudenschleger, D., Ruland, H., Muhler, M., 2020. Identifying the nature of the active sites in methanol synthesis over Cu/ZnO/$Al_{(2)}O_{(3)}$ catalysts. Nat. Commun. 11 (1), 3898.
Li, M., Jiao, L., Nawaz, M.A., et al., 2019. A one-step synthesis method of durene directly from syngas using integrated catalyst of Cu/ZnO/Al_2O_3 and Co-Nb/HZSM-5. Chem. Eng. Sci. 200, 103–112.
Li, S., Guo, L., Ishihara, T., 2020. Hydrogenation of CO_2 to methanol over Cu/AlCeO catalyst. Catal. Today 339, 352–361.
Liang, B., Ma, J., Su, X., et al., 2019. Investigation on deactivation of Cu/ZnO/Al_2O_3 catalyst for CO_2 hydrogenation to methanol. Ind. Eng. Chem. Res. 58 (21), 9030–9037.
Liu, Y.-M., Liu, J.-T., Liu, S.-Z., et al., 2017. Reaction mechanisms of methanol synthesis from CO/CO_2 hydrogenation on Cu_2O(111): comparison with Cu(111). J. CO_2 Util. 20, 59–65.
Mousavi-Kamazani, M., 2019. Facile sonochemical-assisted synthesis of Cu/ZnO/Al_2O_3 nanocomposites under vacuum: optical and photocatalytic studies. Ultrason. Sonochem. 58, 104636.
Okemoto, A., Harada, M.R., Ishizaka, T., et al., 2020. Catalytic performance of MoO_3/FAU zeolite catalysts modified by cu for reverse water gas shift reaction. Appl. Catal. Gen. 592, 117415.
Pampararo, G., Garbarino, G., Riani, P., et al., 2020. A study of ethanol dehydrogenation to acetaldehyde over supported copper catalysts: catalytic activity, deactivation and regeneration. Appl. Catal. Gen. 602, 117710.
Panyad, S., Jongpatiwut, S., Sreethawong, T., et al., 2011. Catalytic dehydroxylation of glycerol to propylene glycol over Cu–ZnO/Al_2O_3 catalysts: effects of catalyst preparation and deactivation. Catal. Today 174 (1), 59–64.
Pasupulety, N., Driss, H., Alhamed, Y.A., et al., 2015. Studies on Au/Cu–Zn–Al catalyst for methanol synthesis from CO_2. Appl. Catal. Gen. 504, 308–318.
Pontzen, F., Liebner, W., Gronemann, V., et al., 2011. Co_2-based methanol and DME – efficient technologies for industrial scale production. Catal. Today 171 (1), 242–250.
Previtali, D., Longhi, M., Galli, F., et al., 2020. Low pressure conversion of CO_2 to methanol over Cu/Zn/Al catalysts. The effect of mg, ca and sr as basic promoters. Fuel 274, 117804.
Rafiee, A., 2020. Modelling and optimization of methanol synthesis from hydrogen and CO_2. J. Environ. Chem. Eng. 8 (5), 104314.
Ren, H., Xu, C.-H., Zhao, H.-Y., et al., 2015. Methanol synthesis from CO_2 hydrogenation over Cu/γ-Al_2O_3 catalysts modified by ZnO, ZrO_2 and MgO. J. Ind. Eng. Chem. 28, 261–267.
Ren, S., Fan, X., Shang, Z., et al., 2020. Enhanced catalytic performance of Zr modified CuO/ZnO/Al_2O_3 catalyst for methanol and dme synthesis via CO_2 hydrogenation. J. CO_2 Util. 36, 82–95.
Sadeghinia, M., Rezaei, M., Nemati Kharat, A., et al., 2020. Effect of In_2O_3 on the structural properties and catalytic performance of the CuO/ZnO/Al_2O_3 catalyst in CO_2 and CO hydrogenation to methanol. Mol. Catal. 484, 110776.
Studt, F., Abild-Pedersen, F., Wu, Q., et al., 2012. CO hydrogenation to methanol on Cu–Ni catalysts: theory and experiment. J. Catal. 293, 51–60.
Sun, K., Fan, Z., Ye, J., et al., 2015. Hydrogenation of CO_2 to methanol over In_2O_3 catalyst. J. CO_2 Util. 12, 1–6.
Tursunov, O., 2017. A brief review of carbon dioxide hydrogenation to methanol over copper and iron based catalysts. Oil Gas Sci. Technol. 72.
Tursunov, O., Kustov, L., Tilyabaev, Z., 2017. Methanol synthesis from the catalytic hydrogenation of CO_2 over CuO–ZnO supported on aluminum and silicon oxides. J. Taiwan Inst. Chem. Eng. 78, 416–422.
Wang, D., Zhao, J., Song, H., et al., 2011. Characterization and performance of Cu/ZnO/Al_2O_3 catalysts prepared via decomposition of m(Cu, Zn)-ammonia complexes under sub-atmospheric pressure for methanol synthesis from H_2 and CO_2. J. Nat. Gas Chem. 20 (6), 629–634.
Wu, Q., To, A.T., Nash, C.P., et al., 2021. Spectroscopic insight into carbon speciation and removal on a Cu/BEA catalyst during renewable high-octane hydrocarbon synthesis. Appl. Catal. B Environ. 287, 119925.
Xiao, S., Zhang, Y., Gao, P., et al., 2017. Highly efficient cu-based catalysts via hydrotalcite-like precursors for CO_2 hydrogenation to methanol. Catal. Today 281, 327–336.
Yang, R., Yu, X., Zhang, Y., et al., 2008. A new method of low-temperature methanol synthesis on Cu/ZnO/Al_2O_3 catalysts from CO/CO_2/H_2. Fuel 87 (4), 443–450.
Yang, X., Meng, Q., Ding, G., et al., 2018. Construction of novel Cu/ZnO-Al_2O_3 composites for furfural hydrogenation: the role of al components. Appl. Catal. Gen. 561, 78–86.
Zhan, H., Gao, P., Zhao, N., et al., 2014. Methanol synthesis from CO_2 hydrogenation over La–M–Cu–Zn–O (m = Y, Ce, Mg, Zr) catalysts derived from perovskite-type precursors. J. Power Sources 251, 113–121.
Zhan, H., Shi, X., Tang, B., et al., 2021. The performance of Cu/Zn/Zr catalysts of different Zr/(Cu+Zn) ratio for CO_2 hydrogenation to methanol. Catal. Commun. 149, 106264.
Zhang, C., Yang, H., Gao, P., et al., 2017. Preparation and CO_2 hydrogenation catalytic properties of alumina microsphere supported cu-based catalyst by deposition-precipitation method. J. CO_2 Util. 17, 263–272.
Zhang, F., Liu, Y., Xu, X., et al., 2018. Effect of al-containing precursors on Cu/ZnO/Al_2O_3 catalyst for methanol production. Fuel Process. Technol. 178, 148–155.
Zhang, L.-X., Zhang, Y.-C., Chen, S.-Y., 2011. Effect of promoter TiO_2 on the performance of CuO-ZnO-Al_2O_3 catalyst for CO_2 catalytic hydrogenation to methanol. J. Fuel Chem. Technol. 39 (12), 912–917.
Zhang, L., Zhang, Y., Chen, S., 2012. Effect of promoter SiO_2, TiO_2 or SiO_2-TiO_2 on the performance of CuO-ZnO-Al_2O_3 catalyst for methanol synthesis from CO_2 hydrogenation. Appl. Catal. Gen. 415–416, 118–123.
Zhuang, Y., Currie, R., Mcauley, K.B., et al., 2019. Highly-selective CO_2 conversion via reverse water gas shift reaction over the 0.5wt% Ru-promoted Cu/ZnO/Al_2O_3 catalyst. Appl. Catal. Gen. 575, 74–86.
Zuo, Z.-J., Wang, L., Han, P.-D., et al., 2014. Methanol synthesis by CO and CO_2 hydrogenation on Cu/γ-Al_2O_3 surface in liquid paraffin solution. Appl. Surf. Sci. 290, 398–404.